Title:

CRIPTO promotes extracellular vesicle uptake and activation of fibroblast exposed to triple negative breast cancer cells

Authors:

David W. Freeman[1,2], Brooke L. Gates[1,2], Mauri D. Spendlove[1], H. Evin Gulbahce[3], Benjamin T. Spike[1,2]

1. Huntsman Cancer Institute, University of Utah, Salt Lake City, UT 84112, USA
2. Department of Oncological Sciences, University of Utah, Salt Lake City, UT 84112, USA
3. Department of Pathology and Laboratory Medicine, Huntsman Cancer Institute, University of Utah Health, Salt Lake City, UT 84112, USA

*Correspondence: Benjamin.spike@hci.utah.edu

Keywords: Breast Cancer, Cancer Associated Fibroblasts, Extracellular Vesicles, CRIPTO, Tumor Microenvironment

ABSTRACT

Expression of CRIPTO, a factor involved in embryonic stem cells, fetal development, and wound healing, is tied to poor prognosis in multiple cancers. In previous models of triple negative breast cancer (TNBC), CRIPTO blockade inhibits tumor growth and dissemination. Here, we describe a novel mechanism by which CRIPTO-laden tumor extracellular vesicles (TEVs) facilitate reciprocal crosstalk between tumor cells and fibroblasts that drives aggressive TNBC phenotypes. CRIPTO expression in TNBC cells was required to program fibroblasts towards a cancer associated fibroblasts cell-state that promoted tumor cell invasion. TEVs bearing CRIPTO increased SMAD2/3 activation and TEV uptake in target fibroblasts through NODAL-dependent and -independent mechanisms, respectively. *In vivo*, CRIPTO levels dictated TEV uptake in the mouse lung, a site of EV-regulated premetastatic niches important for breast cancer dissemination. These discoveries highlight CRIPTO's potential to coordinate heterotypic cellular crosstalk through a previously unrecognized mechanism with implications for development, metastasis, and drug delivery.

INTRODUCTION

Tumors are comprised of an intricate network of parenchymal and stromal cells, whose intercellular signaling dictates cell state change, resistance to therapy, and tumor growth at both primary and distant sites[1]. Deciphering the molecular underpinnings of coordinate heterotypic signaling in these multi-cellular tumor microenvironments (TME) is crucial for understanding tumor progression and could uncover effective therapeutic strategies aimed at non-autonomous drivers of cancer progression and metastasis.

CRIPTO is a small GPI-anchored signaling protein encoded by the *TDGF1* gene that is prominently expressed in stem cells and early development, largely undetectable in adult homeostatic tissue, but reexpressed in the context of oncogenesis and wound healing[2]. In mammary developmental studies, inhibition of CRIPTO with a soluble CRIPTO ligand trap, Alk4^{L75A}-Fc (A4Fc), significantly impaired the multipotency of murine mammary stem cells and their proliferative renewal capacity[3]. Elevated CRIPTO is detectable in nearly 80% of breast cancers and its overexpression in upwards of 50% of invasive breast tumors is associated with poor prognosis and advanced disease states[4,5]. Knocking down CRIPTO, blocking its signaling with A4Fc, or delivering toxic payloads to CRIPTO expressing cells with an antibody-drug conjugate reduces primary tumor growth and distant metastasis in triple negative breast cancer (TNBC) xenograft models[6,7].

CRIPTO signaling is multifaceted[2,8]. It acts as a pivotal intermediary in cellular signaling by modulating the TGF-β pathway and independent pathways that activate c-Src/MEK/AKT[9]. In TGF-β signaling, it acts as an obligate co-receptor for the TGF-β family ligand NODAL while attenuating ACTIVIN and TGF-β1 activity[10-12]. Mechanisms of CRIPTO's growth factor-like signaling remain to be clarified. CRIPTO signaling is potentiated by direct interaction with cell-

surface GRP78[13]. During periods of cellular stress, a fraction of GRP78 relocalizes from the endoplasmic reticulum – where it functions as a key regulator of the unfolded protein response – to the cell surface. This relocalization positions CRIPTO signaling as part of a microenvironment-responsive signaling axis. Within breast cancer xenograft models, we have shown CRIPTO and GRP78 co-localize along stressed hypoxic tumor margins, where A4Fc inhibits cell proliferation[7].

Though CRIPTO is known to act both autonomously *and* as a soluble secreted factor, it has been studied in cancer primarily as an autonomous factor within the epithelial tumor parenchyma. However, there is good reason to suspect CRIPTO may coordinate the activity of multiple cooperating cell types. Patients with cirrhotic livers have elevated levels of CRIPTO and alpha-smooth muscle actin (αSMA) expression, and similar patterns are seen in fibrotic remodeling after myocardial infarction[14]. We previously showed CRIPTO is distributed throughout the stromal environment in developing mammary rudiments, and is a crucial mediator of augmented proliferative potential of mammary stem cells when co-cultured with fibroblasts, suggesting a broader regulatory role in multicellular cooperation during tissue morphogenesis[3].

The interaction of heterotypic cells is critical in cancer. For instance, breast cancer associated fibroblasts (CAFs) facilitate treatment resistance, tumor proliferation, and enable metastatic outgrowth, partly through mechanical alterations of the ECM and cytokine secretion. They are one of the most abundant cell types in the tumor microenvironment (TME) and are thought to originate primarily from resident mammary fibroblasts, with potential contributions from mesenchymal stem cells[1]. The diversity of CAFs is influenced by molecular and pathological subtypes, intratumor spatial patterning, and microenvironmental cues like hypoxia. Though critical aspects of their interactions with parenchymal tumor cells hold high potential for

therapeutic manipulation, the interactions are complex, and key targetable regulators remain to be identified[15-17].

Here, we demonstrate that CRIPTO governs a novel communication axis between tumor cells and fibroblasts involving extracellular vesicles (EVs). This discovery emerged from our analysis of single cell profiles of the TNBC cell line, MDA-MB-468. Specific subpopulations of MDA-MB-468 cells were found to be CRIPTO dependent and correlate with CAF levels in patients, though the signatures are distinct from classic EMT or CAF signatures. Enriched gene categories included vesicular trafficking and extracellular vesicle programs. Together, these observations prompted us to evaluate CRIPTO-mediated tumor cell-fibroblast crosstalk and the potential role of EVs.

EVs are secreted mediators of intercellular crosstalk capable of shuttling proteins, DNA/RNA, lipids, and various metabolites. Classically, EVs have been divided into three classes: (1) Exosomes formed through endocytic intermediates, (2) Microvesicles produced through outward membrane blebbing, and (3) Apoptotic bodies generated from dying cells[18]. Roles for EVs in tumor initiation and progression have been described, including their capacity to prime pre-metastatic niches in distant organs for tumor cell colonization[19]. We demonstrate that tumor cell derived CRIPTO can foster fibroblast programming through paracrine signaling via extracellular vesicles (EVs).

Mechanistically, CRIPTO-laden EVs can activate NODAL signaling in target fibroblasts while exhibiting elevated NODAL-independent EV uptake *in vitro,* as well as elevated uptake in lungs of mice where EVs have been implicated in the formation of pre-metastatic niches through fibroblast modification. This discovery represents a key milestone in understanding CRIPTO

activity in multicellular contexts, including tumor microenvironments where CRIPTO-dependent EV signaling could represent a novel therapeutic target for breast cancer and beyond.

RESULTS

Tumor cell derived CRIPTO activity correlates with cancer associated fibroblast (CAF) levels and patient outcomes

We previously showed that CR1 antagonism by A4Fc limits various phenotypes in TNBC cells associated with stemness and tumor progression, including the capacity of TNBC (MDA-MB-468) organoids to undergo serial passaging without overt pre-passage organoid phenotypes[7]. This suggested CRIPTO may regulate the maintenance of a stem-like cell population required for secondary organoid outgrowth[7]. To test this, we performed single cell RNA-sequencing (scRNA-seq) of MDA-MB-468 organoids transduced with an empty tet-inducible lentiviral expression cassette ($s14^{Con}$) or a construct with inducible expression of secreted A4Fc ($s14^{A4Fc}$). Inhibition of CRIPTO with A4Fc induced a marked skewing in two specific cell subpopulations (denoted cluster 5 and 8) (**Fig 1A)**. $s14^{A4Fc}$ cultures showed a marked loss of cluster 8 cells and an increase in cluster 5 cells relative to $s14^{Con}$ cultures. We identified differentially expressed genes (DEGs) representing these populations and confirmed CRIPTO dependency of select targets using *TDGF1* knockdown (shCr) (**Fig 1B,C)**.

To help identify underlying biology regulated by CRIPTO in this setting, we examined the enrichment of DEGs associated with these subpopulations in curated biological processes and cellular compartment gene sets. Genes characteristic of cluster 8 showed enrichment in factors predicted to localize to extracellular vesicles (EV) and exosomes **(Fig 1D, Fig S1A,B)**. Though somewhat unexpected based on CRIPTO's role as a cell surface co-receptor, this link between CRIPTO and EV biology was consistent with punctate staining we previously observed for CRIPTO in tumor and developmental settings[3], unpublished proteomics work from our group

analyzing A4Fc pulldowns from xenografts indicating associated EV-markers, and recent reports of CRIPTO expression in EVs from cholangiocarcinoma patients[7,20].

Given the role of EVs as critical signaling mediators between tumor cells and tumor-supportive stroma, we investigated whether EVs drive 'call and response' programs between CRIPTO-regulated tumor cell populations and TME cell types[19,21]. First, we generated a composite gene signature (CRIPTO Signature) for cluster 8 and cluster 5 reflecting tumor cell states under CRIPTO's influence and assessed its correlation with TME cell populations using TCGA data (**Fig 1E, Table S1**)[22,23]. The CRIPTO signature was overexpressed in TNBC relative to other subtypes and among stromal signatures in the TCGA database, was most strongly correlated with a CAF gene signature, an association that persisted even after adjusting for the modest number of shared genes between the signatures and proliferation-related genes (**Fig 1E-G; Fig S1C-E)**. These findings are consistent with a CRIPTO-regulated tumor subpopulation influencing stromal fibroblast programs within the TME.

CRIPTO drives EV uptake by recipient fibroblasts

Recent studies have identified CRIPTO in tumor-derived EVs (TEVs) in several cancer types[20,24]. To determine whether CRIPTO was likely to be present in EVs within the TME of breast cancers in our system, we reanalyzed MDA-MB-468 xenograft tumors for expression and localization of CRIPTO and the canonical EV marker CD81[25]. CRIPTO colocalized with CD81 in discrete punctate structures along hypoxic tumor borders of MDA-MB-468 xenografts, where we previously observed CRIPTO-dependent tumor cell phenotypes (**Fig 2A**)[7].

Indeed, isolated EVs from conditioned media of shCon MDA-MB-468 *in vitro* cultures exhibited no obvious difference in canonical EV markers, size distribution, production quantity, or morphology from EVs isolated from shCr cultures (**Fig 2B-D**). Nevertheless, timelapse

microscopy of s14^{Con}- and s14^{A4Fc}-expressing fibroblasts treated with fluorescently labeled TEVs produced from shCon or shCr MDA-MB-468 cells demonstrated marked differences in EV uptake. shCr EVs were internalized at lower rate compared to shCon in s14^{Con} cells and expression of A4Fc in recipient fibroblasts reduced the uptake of shCon EVs (**Fig 2E**).

We next asked whether CRIPTO regulates EV uptake *in vivo* in mouse lungs where premetastatic niches governed by EVs have been described and where we previously saw a drastic reduction in metastasis of the TNBC cell line MDA-MB-231 when CRIPTO was blocked by A4Fc[7,19]. Thus, we performed retroorbital injections of PKH26-labeled EVs isolated from shCon and shCr MDA-MB-231 cells and analyzed lung tissue 24 hours later. We observed EV uptake by rare cells throughout the lung in each case but noted that EVs from shCr cells exhibited significantly lower levels of uptake in the lungs than EVs from shCon cells (**Fig 2F,G**). Collectively, these data point towards a previously unidentified role for CRIPTO in enhancing EV uptake.

Paracrine CRIPTO signaling promotes reciprocal tumor:fibroblast crosstalk

To understand the effects of paracrine CRIPTO signaling via EVs on fibroblast activity, we first reexamined TNBC xenograft tumors expressing s14^{Con} of s14^{A4Fc} in which we had originally reported effects of A4Fc on tumor cell aggressiveness and disease progression, focusing now on the TME rather than the tumor parenchyma[7]. Consistent with a role for CRIPTO in regulating CAF activity, we noted alterations in collagen deposition under CRIPTO inhibition by A4Fc and qualitative changes in stromal cell morphology and expression of αSMA (**Fig. S2A-B**). Similarly, PDX models showing greater enrichment for the CRIPTO signature also scored higher for overall fibrosis (**Fig 3A,B**), collectively suggesting a functional relationship between CRIPTO signaling and CAF activity.

To functionally interrogate CRIPTO-dependent coordination of tumor cell and fibroblast interaction in a controlled setting, we generated heterotypic organoid co-cultures of MDA-MB-468 cells and growth-arrested 3T3 fibroblasts expressing $s14^{Con}$ or $s14^{A4Fc}$ In microwell cultures, incorporation of $s14^{Con}$-fibroblasts stimulated tumor cell and fibroblast co-migration out of the well nadir, whereas A4Fc expression reduced tumor cell migration despite no appreciable difference on fibroblast movement (**Fig 3C**). Related experiments using transwell invasion assays confirmed that the migratory phenotype in tumor cells was at least partly driven by soluble paracrine signaling and involved tumor cell-dependent reprogramming of fibroblast cell state for reciprocal promotion of tumor cell migration. That is, when naïve tumor cells were cultured above either naïve $s14^{Con}$ or $s14^{A4Fc}$ fibroblasts over 48hrs, they migrated through Matrigel and the boundary membrane at low and comparable rates. However, primed fibroblasts (i.e. those previously exposed to tumor cells for a period of 3 days) dramatically enhanced the invasion of naïve tumor cells over 48 hours, and this was significantly reduced by A4Fc (**Fig 3D**). This migratory effect extended to organoid cultures of Patient Derived Xenografts (PdxOs) that endogenously expressed CRIPTO at different levels (**Fig 3D-E, Fig S2C**).

We also examined canonical CAF markers by RT-qPCR following treatment of 3T3 fibroblasts with tumor cell conditioned media (CM). Repeated treatment with CM for 3 days from shCon cells altered the expression of CAF markers relative to fibroblasts treated with autologous conditioned media, whereas these changes were attenuated when treating with CRIPTO knockdown CM (**Fig 3F**). Together, these data indicate tumor cell CRIPTO is indispensable in directing fibroblast reprogramming through soluble paracrine signaling.

EVs facilitate fibroblast activation through intercellular CRIPTO:NODAL signaling

We next examined TEVs as possible mediators of paracrine CRIPTO signaling and fibroblast programming. SMADs play a key role in CAF activation and are regulated by various TGF-β

family ligands and CRIPTO[12,26]. We, therefore, investigated SMAD2/3 activation in fibroblasts as a function of paracrine signaling by CRIPTO-bearing TEVs. Conditioned media from control MDA-MB-468 cells potently induced SMAD2/3 phosphorylation in fibroblasts, and the activity was specifically associated with the isolated EV fraction of the control cell CM, while it was absent from EV depleted fractions and from both fractions of EVs isolated from shCRIPTO cells (**Fig 4A**). This implicates TEVs as the predominant signaling mechanism mediating non-autonomous CRIPTO signaling between tumor cells and fibroblasts.

CRIPTO acts through ALK4 in conjunction with various TGF-β family ligands to modulate SMAD2/3 activation[11]. We confirmed the invovment of ALK4,5,7 receptor complexes in CRIPTO mediated SMAD2/3 activation in fibroblasts using pharmacological inhibition (SB431542). ALK4,5,7 inhibition in fibroblasts blocked pSMAD2/3 increases following treatment with shCon TEVs (**Fig 4B**).

CRIPTO-mediated activation of SMAD2/3 typically involves the TGF-β family ligand NODAL and NODAL has previously been associated with active CAFs in TNBC[27]. We asked whether CRIPTO-expressing TEVs promoted SMAD2/3 activation by facilitating signaling through locally produced NODAL in fibroblasts. We found NODAL knockdown (shNODAL) in recipient fibroblasts blocked SMAD2/3 phosphorylation in fibroblasts treated with TEVs from CRIPTO expressing TNBC cells (**Fig 4C**). These data suggested a model in which tumor cells provide CRIPTO to fibroblasts in the form of CR-laden EVs that then act in concert with fibroblast-expressed NODAL to program fibroblasts to reciprocally promote tumor cell migration. Consistent with this conjecture, fibroblasts treated with isolated shCon TEVs promoted tumor cell invasion and this effect was reversed by knockdown of CRIPTO in the EV-producing tumor cells or by NODAL knockdown in the recipient fibroblasts (**Fig 4D**). These data highlight an

intercellular signaling axis dependent on CRIPTO and NODAL expression in separate cell populations.

We next asked whether TEV uptake was contingent on NODAL expression within fibroblasts. Fluorescently labeled TEVs from shCon cells were taken up equally by control and shNodal fibroblast while TEVs from shCr cells were internalized less readily, regardless of NODAL expression in fibroblasts. In contrast, levels of nuclear SMAD2/3 (indicative of SMAD activation) were dependent on both fibroblast NODAL levels and tumor CRIPTO levels (**Fig 4E**). Critically, the differential EV uptake observed in our 3T3 model system was recapitulated using primary human mammary fibroblasts as the recipient cell type. In primary human fibroblasts, shCon EVs were taken up more readily than shCr EVs and promoted nuclear localization of SMAD2/3 that was diminished when using shCr-donor cell EVs (**Fig 4E**). Thus, CRIPTO regulates EV uptake and SMAD activation through distinct pathways in fibroblasts. Interestingly, patient-derived CAFs showed trends of enhanced TEV uptake from CRIPTO-expressing cells relative to shCR TEV that were similar to 3T3s, though not statistically significant. However, we observed comparable levels of nuclear SMAD localization (indicative of activation) in CAFs treated with shCon TEVs versus those treated with shCr TEVs (**Fig 4F**). Suggesting CAFs, as opposed to normal resident fibroblasts, may have activated secondary mechanisms to sustain SMAD activation independently of CRIPTO-TEV signaling (**Fig 4F**).

DISCUSSION

In the TME, non-autonomous signaling drives adaptive responses in both stromal and parenchymal cells, contributing to cancer progression and resistance to treatment[1,16]. Our study uncovers a novel instructive role for tumor cell-derived EVs bearing CRIPTO protein in this dynamic activity. CRIPTO-laden EVs program fibroblasts toward an activated fibroblast cell-state, which in turn enhances tumor cell invasion. This process involves NODAL-dependent

activation of SMAD2/3 in recipient fibroblasts and CRIPTO-dependent but NODAL-independent EV uptake.

Our prior studies point to stress-dependent activation of CRIPTO signaling in parenchymal cells enhancing tumor cell fitness as a function of GRP78 cell surface localization within stressed tumor microdomains[7]. We show here that such domains also exhibit colocalization of CRIPTO with EV marker CD81 and correlated increases in elongated, αSMA-positive fibroblasts and fibrosis. Chronic exposure of fibroblasts to CRIPTO-bearing EVs drives SMAD activation, the expression of classical CAF markers, and transcriptional changes associated with the TGF-β pathway, matrisome remodeling, and ER stress.

Whether CRIPTO's role in autocrine/paracrine signaling via EVs involves the packaging of other pathway components as EV cargo remains to be determined. EVs are known to promote αSMA expression in fibroblasts by transferring latent TGF-β complexes from tumor cells[21]. Furthermore, CRIPTO not only facilitates NODAL ALK4 complex formation, but also regulates proper NODAL localization and trafficking via coupling with convertases FURIN and PACE4[28,29]. In addition to TGF-β pathways, CRIPTO influences growth factor signaling through c-Src and ERK/AKT pathways[9]. The promotion of ERK activation in target fibroblast cells by non-EV-specific soluble factors that is blocked by CRIPTO-EVs suggests a multifaceted cooperation between cell types and signaling pathways. The restoration of ERK activation by inhibiting ALK4,5,7 indicates EV-based CRIPTO may balance differentiation and proliferation cues to facilitate CAF activation.

Our initial indication of CRIPTO's role in modulating fibroblast behavior stems from a correlation between a CAF signature and the prevalence of CRIPTO-regulated tumor populations. This suggests that these tumor populations are key players in the complex interplay of signals between CAFs and tumor cells, highlighting the importance of understanding tumor cell heterogeneity and the nuanced "call and response" mechanisms driving tumor

progression. We also noted the correlation of CRIPTO populations with a $CD4^+$ T cell signature. The basis of this relationship will require further investigation, but we note that CAFs have been reported to alter intratumoral immune cell levels through cytokine secretion and alteration of the mechanical profile of the extracellular matrix[30,31]. Whether CRIPTO activity influences immune components of the TME directly or through altered CAF activity presents intriguing avenues for future research, especially regarding CRIPTO inhibition's potential synergy with immune checkpoint blockade.

Our study utilizes various cell lines and patient-derived TNBC models highlighting elevated CRIPTO activity in this subtype. However, the findings are potentially relevant to other breast cancer subtypes or cancers in other tissues with significant fibroblast involvement, such as lung, liver, prostate, and pancreatic cancer. Indeed, CRIPTO overexpression has been reported in a broad spectrum of breast cancers, including hormone receptor (HR+) and HER2+ tumors in addition to TNBC[5]. Further, CRIPTO/GRP78 signaling has now been implicated in an array of tumor types outside of the mammary system[32,33].

EVs from MDA-MB-231 sublines prime pre-metastatic niches, specifically targeting cells, including S100A4+ lung fibroblasts through differential integrin expression[19]. Here we report for the first time that modulation of CRIPTO expression in tumor cells significantly changes EV uptake rates and cellular programming of recipient cells both *in vitro* and *in vivo*. This discovery of may open new avenues for therapy development by blocking critical CRIPTO-EV's role in modifying stromal fibroblasts. Previous efforts to target the tumor microenvironment (TME) and CAFs in breast cancer, particularly using TGF-β inhibitors, have failed early clinical trials due to significant off-target toxicities[34]. In contrast, CRIPTO, minimally expressed in normal adult tissue, could present a safer target, with previous *in vivo* targeting showing no adverse effects[7,35]. This could be especially valuable in the TNBC subtype that currently has limited targeted therapies, with significant implications for developingt therapies.

In conclusion, our study establishes CRIPTO as a pivotal component of heterotypic tumor:fibroblast signaling within TNBC, with potential biologic and therapeutic relevance to other cancers via its role in modulating EV internalization and signaling within the TME. While significant advances have been made in targeting the immune stromal component of the microenvironment, limited inroads have been made in targeting CAFs in breast cancer despite their prevalence and critical roles. By targeting tumor-supportive CAFs, it may be possible to dampen mechanisms of resistance, and therefore, CRIPTO-directed therapies may prove to be important players in combinatorial therapeutic approaches. Collectively, these data have implications for biomarker and therapeutic target discovery.

METHODS

Cell culture

MDA-MB-468, MDA-MB-231 and NIH-3T3 cells were acquired from ATCC. Cells were cultured in 'Tumor Media' (Dulbecco's modified Eagle's media (DMEM), 10% fetal bovine serum, and ciprofloxacin 10μg/mL). NIH-3T3 cells were treated with 1μg/mL of mitomycin-C for 2 hours to generate growth arrested fibroblasts. For treatments with inhibitors or EVs, cells were cultured with media containing EV-depleted FBS for 24 hours prior to treatment. PDxOs were a generous gift from the Welm Labs (HCI) and were cultured according to their published protocol[36]. Primary human mammary fibroblasts and CAFs were aquired from Cell Biologics and cultured in tumor media tumor media supplemented with FGF (100ng/mL) and hydrocortisone (1μg/mL).

RNA-sequencing

For scRNA-seq MDA-MB-468 expressing either s14-Con or s14-A4 were grown as organoids in low adhesion plates with 5% Engelbreth-Holm-Swarm (EHS)-derived basement membrane matrix for 7 days. Organoids were trypsinized, dissociated with dispase and barcoded with the

Chromium Next GEM Single Cell 3' Kit v3.1 with cell multiplexing according to the manufacturer's instructions [Protocol #1] (#100261, 10X Genomics, Pleasanton, CA). Sequencing was performed on the NovaSeq 6000 with 150x150 paired end mode by the University of Utah High Throughput Genomics Core (HTGC) at Huntsman Cancer Institute based on the 10X genomics user guide (CG000315).

For bulk RNAsequencing, NIH/3T3s were cultured in EV-depleted tumor media and treated with 2.5μg of purified EVs from MDA-MB-468 shCon, shCripto, or CRIPTO overexpressing cells for 24 hours. RNA was collected with RNeasy Kit according the manufacturer's instructions (#74104, Qiagen, Germantown, MD) and purity was validated using a 2100 Bioanylyzer (Agilent Technologies, Santa Clara, CA) and Qubit™ Broad Range RNA kit (Thermo Fisher Scientific, Waltham, MA). Libraries were prepped with the NEBNext Ultra II Directional RNA library Prep with Poly(A) isolation (New England Biolabs, Ipswich, MA). Reads were aligned to the mouse genome using Elysium. We quantified gene expression as transcripts per million (TPM).

Lentiviral Vectors:

S14-Con and -A4 lentiviral expression vectors are previously described tet-inducible constructs[7]. *TDGF1* and *NODAL* knockdown constructs were purchased from Horizon Discovery and Origene respectively.

Immunofluorescence

Cells were cultured on 8-well chamber slides with removable covers (#155409PK, Thermo Fisher Scientific, Waltham, MA). Upon culture endpoint cells were fixed with 4% PFA, permeabilized with 0.05% Triton-X 100, and blocked with 10% goat serum. For EV internalization, cells were incubated with 1μg of PKH26-labeled EVs for 1 hour prior to fixation.

Permeabilized cells were probed for SMAD2/3 (#AF3797, R&D Biosystems, 10μg/mL) and imaged on an SP8 white laser confocal microscope (Leica Biosystems, Wetzlar, Germany).

Microwell Organoid Assay

MDA-MB-468 and mitomycin-C treated NIH-3T3 cells were plated at a ratio of 10:1 in AggreWell™400 plates at approximately 50 cells/microwell according to the manufacturer's instructions (#34415, Stemcell Technologies, Vancouver, BC) and grown for 5 days in tumor media containing 1μg/mL doxycycline. Dispersed cell counts were measured blinded as the number of cells present beyond the average diameter of MDA-MB-468 monoculture spheroids using the image analysis software FIJI[37].

Western Blots

Cells and EVs were lysed in RIPA buffer supplemented with protease/phosphatase inhibitors (#78440, Thermo Fisher Scientific, Waltham, MA) and quantified with DC Protein Assay (#500111, BioRad, Hercules, CA). Lysates were boiled in LDS loading buffer with 0.1M DTT and run on 4-12% precast Bis-Tris gels (NP0336BOX, Thermo Fisher Scientific, Waltham, MA). Proteins were transferred using an iBlot2 transfer device (Thermo Fisher Scientific, Waltham, MA), blocked with Intercept Blocking Buffer (927-7001, LiCor Biosciences, Lincoln, NE), and immunoblotted with the following antibodies: phospho-SMAD2 (Ser465/467)/SMAD3 (Ser423/425) (Clone D27F4, Cell Signaling, 1:1000), SMAD2/3 (#AF3797, R&D Biosystems, 0.5μg/mL), Phospho-ERK1/2 (Thr202/204) (Clone D13.144E, Cell Signaling, 1:1000), ERK1/2 (L34F12, Cell Signaling, 1:2000), Vinculin (Clone EPR8185, Abcam, 1:1000), Calnexin (Clone C5C9, Cell Signaling, 1:1000), HSP70 (#4872, Cell Signaling, 1:1000), Flotillin-1 (Clone D2V7J, Cell Signaling, 1:1000), CD81 (Clone D3N2D, Cell Signaling, 1:1000), NODAL (Clone WS65, Santa Cruz Biotechnology, 1:200), Goat anti-rabbit IgG AF680 (#A21076, Thermo Fisher

Scientific, 1:2000), Donkey anti-goat IgG AF800 (#A32930, Thermo Fisher Scientific, 1:2000), Goat anti-mouse IgG (#A11375, Thermo Fisher Scientific, 1:2000).

PCR

RNA was isolated from cells using the RNeasy Kit (#74104, Qiagen, Germantown, MD) and quantified on a NanoDrop 8000 (Thermo Fisher Scientific, Waltham, MA). RT-qPCR was performed using PowerUp™ Sybr™ Green Master Mix (#A25741, Thermo Fisher Scientific, Waltham, MA) according to manufacturer's protocol and utilized a BioRad™ CFX384 thermocycler. Comparisons were made using the following pre-validated housekeeping genes: *POLR2A* (Hs.PT.39a.19639531; IDT, San Diego, CA); *Polr2a* (MM.PT.39a.22214849; IDT, San Diego, CA). The following custom RNA-specific primer sequences were designed: *TDGF1:* (Forward: TCCTTTTGTGCCTGCCCTC Reverse: CACAGGGAACACTTCTTGG); *SOSTDC1* (Forward: TCAAGCCAGAAATGGAGGCAGG Reverse: GCCATCAGAGATGTATTTGGTGG); *CRYAB* (Forward: ACTTCCCTGAGTCCCTTCTACC Reverse: GGAGAAGTGCTTCACATCCAGG); *Tnc* (Forward: GAGACCTGACACGGAGTATGAG Reverse: CTCCAAGGTGATGCTGTTGTCTG); *TGF-β* (Forward: TGATACGCCTGAGTGGCTGTCT Reverse: CACAAGAGCAGTGAGCGCTGAA); *S100a4* (Forward: AGCTCAAGGAGCTACTGACCAG Reverse: GCTGTCCAAGTTGCTCATCACC); *Pdgfrα* (Forward: GCAGTTGCCTTACGACTCCAGA Reverse: GGTTTGAGCATCTTCACAGCCAC); *Fn1* (Forward: CCCTATCTCTGATACCGTTGTCC Reverse: TGCCGCAACTACTGTGATTCGG); *Fap* (Forward: CCCGCGTAACACAGGATTCACT Reverse: CACACTTCTTGCTCGGAGGAGA); *Acta2* (Forward: CACTATTGGCAACGAGCGC Reverse: CCAATGAAGGAAGGCTGGAA).

Invasion Assays

Invasion assays were performed using 6.5mm polycarbonate membrane Transwell® inserts with 8.0μm pores. Inserts were coated with 45μL of EHS basement membrane matrix and solidified at 37C for 5 minutes[38]. $2.0x10^4$ tumor cells plated in 100 μL on top of the EHS coated insert were grown with fibroblasts for 72 hours to prime fibroblasts. Priming inserts were discarded and fresh EHS coated inserts with $2.0x10^4$ tumor cells were placed on top of both naïve and primed fibroblasts and cultured for an additional 48 and 72 hours for cell lines and PDxOs, respectively. Inserts were washed with PBS, fixed with 4% PFA for 15 minutes at RT, permeabilized with 0.05% Triton X-100, incubated with DAPI 1 μg/mL for 5 minutes. EHS matrix/non-migrated cells were removed from the top of the transwell with a cotton tipped applicator following permeabilization. Membranes were excised, mounted, and coverslipped in ProLong™ Gold mounting media (#P36930, Thermo Fisher Scientific, Waltham, MA), and imaged on an Axioscan 7 Slide Scanner (Zeiss, Oberkochen, Germany). Membrane area was manually measured and DAPI counts were performed using the automated cell counting program in QuPath[39].

Extracellular Vesicle Isolation and labeling

EVs were isolated by differential ultracentrifugation as previously described and validated according to recent MISEV2023 guidlines[25,40]. Cells were cultured at 70-90% confluency for 48 hours in Tumor Media with EV-depleted FBS. Conditioned media was collected and subjected to sequential centrifugation at 500g for 10 minutes, 2500g for 20 minutes, 10000g for 30 minutes, passed through 0.2μm PES filters and centrifuged at 120,000g for 2 hours (SW28 rotor, K=246). Pelleted EVs were resuspended in 0.2 μm filtered PBS and centrifuged at 120,000g for 2 hours (SW55Ti rotor, K=48). The resulting EV pellet was resuspended in either filtered PBS or RIPA depending on downstream assays. For PKH26 staining, isolated EVs were labeled according to the manufacturer's instructions (MIDI6-1KT, Sigma, Burlington, MA). Excess PKH was removed

by centrifugation at 190,000g for 2 hours with a 0.971M sucrose cushion (SW55Ti rotor, K=48). EVs were resuspended in 9mL of PBS and filtered with a 10kDa centrifugal filter (UFC901008, Sigma, Burlington, MA) at 3000g for 30 minutes. PKH26 labeled EVs were stored at 4C and used within 24 hours of labeling.

Nanoparticle Tracking Analysis

EV samples were diluted 1:20 with 0.2µm filtered PBS. Size distribution and concentration were analyzed on a NS300 (Malvern, Malvern UK). Samples were recorded blinded over 3 videos of 60s at detection threshold: 3, camera level: 13 with a coefficient of variance of <15%.

Electron Microscopy

EVs were applied (3.5 µL) to glow-discharged 2/1 Quantifoil carbon 300-mesh Cu grids. Grids were blotted for 4-6 seconds on the front-side of the grid and immediately plunged into liquid Ethane using a Leica plunge freezing device.

EV Uptake Timecourse

Cells were grown in 8 well chambered coverglass (#155409, Thermo Fisher Scientific, Waltham, MA) and imaged with an SP8 white laser confocal (Leica Biosystems, Wetzlar, Germany) with a stage top incubator (Okolab, Sewickley, PA). Two images per well were taken at 200X magnification in 20 minutes intervals over an 8 hour period. 1µg of PKH26-labeled EVs were added after an initial image and fluorescence intensity was normalized based on the fluorescent EV signal after the secod timepoint for each condition.

In Vivo Studies

10-12 week old SCID-Beige mice were purchased from Charles River Laboratory (Wilmington, MA). All animal care and procedures were approved and monitored by an Institutional Animal Care and Use Committee. For EV uptake studies, mice received retroorbital injections of 10μg of PKH26 (MIDI6-1KT, Sigma, Burlington, MA) labeled EV as previously described[19]. 24 hours following EV administration, animals were euthanized, and lungs and livers were harvested, fixed in 4% PFA overnight followed by sequential incubation in 10% sucrose (1 hour), 20% sucrose (1 hour), and 30% sucrose (overnight) solutions. Fixed tissues were embedded in O.C.T, frozen, and cryosectioned at 5μm.

ACKNOWLEDGMENTS

We would like to thank the cell imaging, electron microscopy, and high throughput genomics cores at HCI for their expertise and equipment, and R. O'Connell for generous use of the nanosight.

AUTHOR CONTRIBUTIONS

Concept and writing: DWF and BTS wrote the manuscript with input from all the authors. DWF and BTS conceived and designed the study, and DWF and BLG conducted the experiments. HEG and MDS performed blinded analysis of PDX sections and microwell assays, respectively.

FUNDING

Portions of this work were supported by the Department of Defense BCRP (BC201559), the Huntsman Cancer Foundation, an NIH-NICHD training grant (T32HD007491) and an NIH CCSG support grant (P30 CA42014). The content is solely the responsibility of the authors and does not necessarily represent the official views of the NIH.

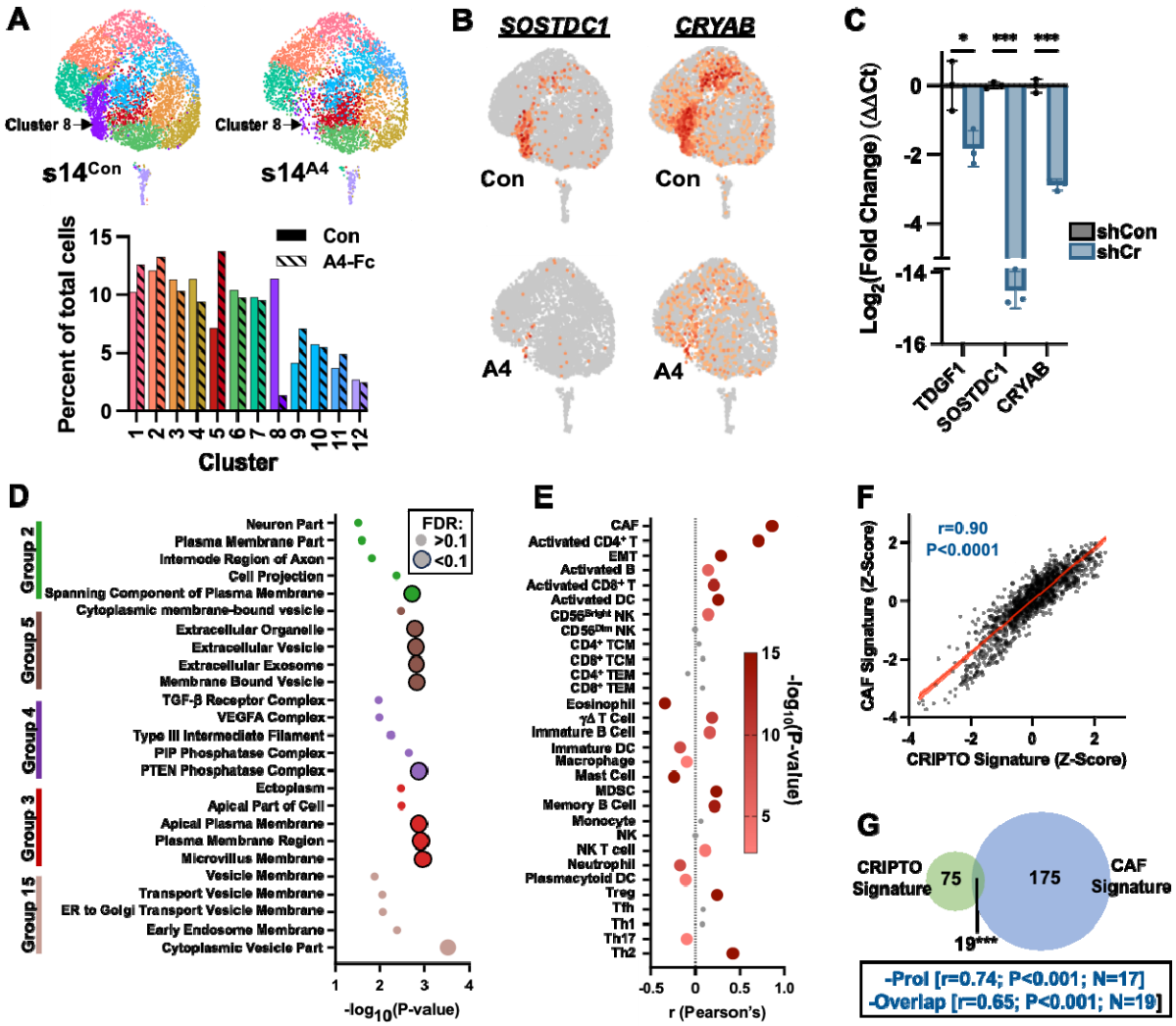

Figure 1. CRIPTO regulates TNBC tumor cell populations associated with extracellular vesicles and CAFs

(A) UMAPS and relative cluster proportions of scRNA-seq of MDA-MB-468 s14^{Con} and s14^{A4Fc} organoids. (B) Representative genes enriched in cluster 8 and (C) validated by RT-qPCR in MDA-MB-468 shCon and shCr 2D cultures; Holm-Šidák Multiple T-tests. (B) Jensen cell compartment analysis of cluster 8 DEGs. Common compartments are clustered together, top 5 compartments for each enriched cluster are shown. Larger bubbles represent significantly enriched compartments (q<0.1; Benjamini-Hochberg). (E) Pearson's correlation of CRIPTO signature with stromal cell type gene signatues, larger bubbles represent significant correlations (Bonferonni adjusted P<0.0017) (H) Pearson's correlation between TDGF1 signature and CAF signature (TCGA). (I) Overlap of genes between CAF and gene signature (Hypergeometric distribution). Resulting Pearson correlations and P-values when genes in common or gene annotated as 'proliferation' by GO analysis were removed from the TCGA and CAF signatures. *P<0.05, ***P<0.001

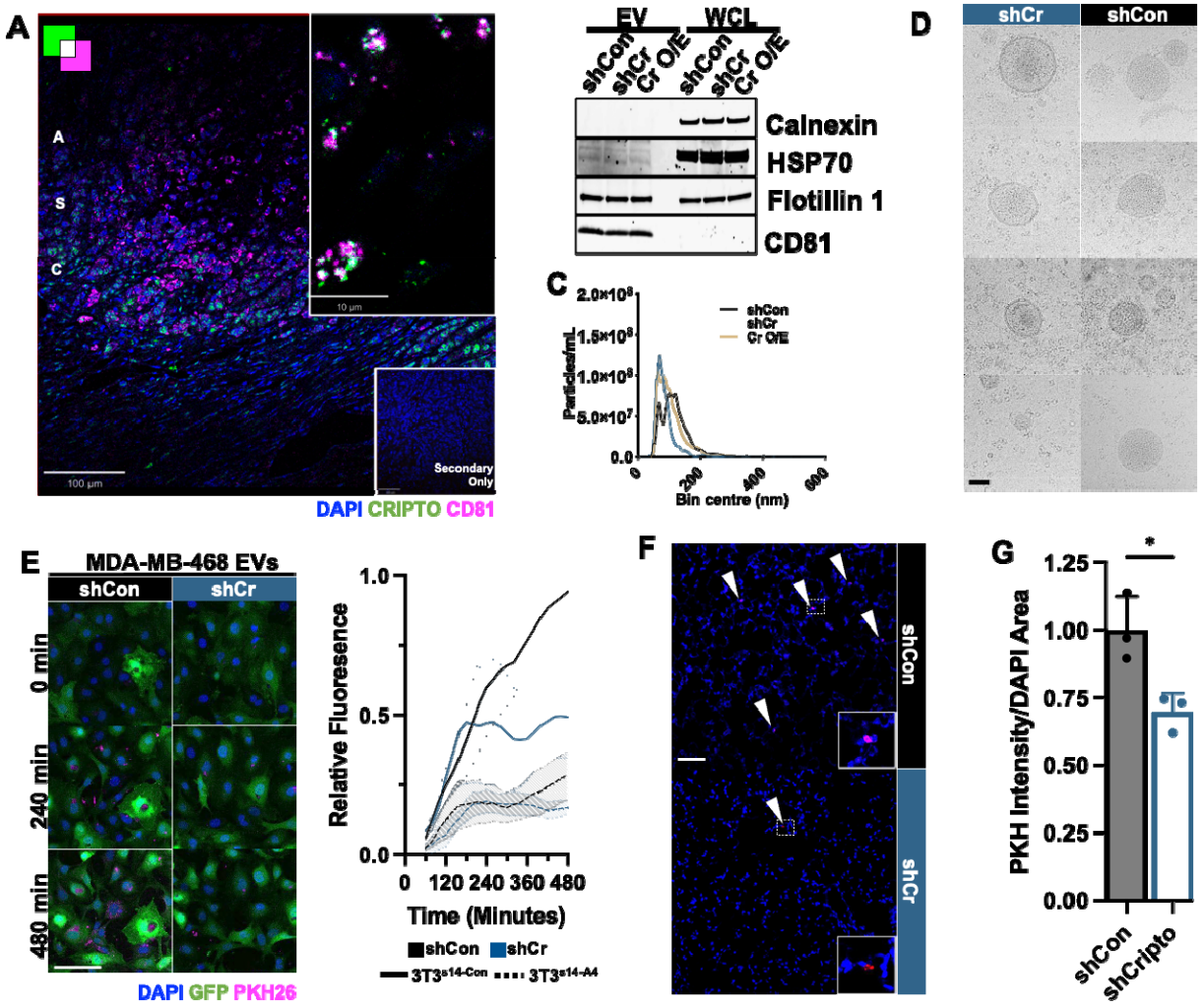

Figure 2. CRIPTO promotes EV uptake *in vitro* and *in vivo*
(A) Immunofluorescence of CD81 and CRIPTO in MDA-MB-468 xenograft tumor; A= acellular, S= stressed and C= cellular. Purity of TEVs isolated from MDA-MB-468 shCon and shCr by (B) Western blot, (C) Nanoparticle tracking analysis and (D) Cryo-electron microscopy, scale bar = 50nm. (E) Representative images and moving average intensity of $3T3^{s14\text{-}Con}$ or $3T3^{s14\text{-}A4}$ cells treated with TEVs from MDA-MB-468 shCon or shCr cells Scale Bar=100µm. (F) Representative images and (G) Quantification of PKH intensity/cell of lungs from mice treated with either PKH26 labeled EVs isolated from shCon, or shCr cells (N=3 animals/group; 5 field of views/animal). Two-tailed student's T-test, *P<0.05.

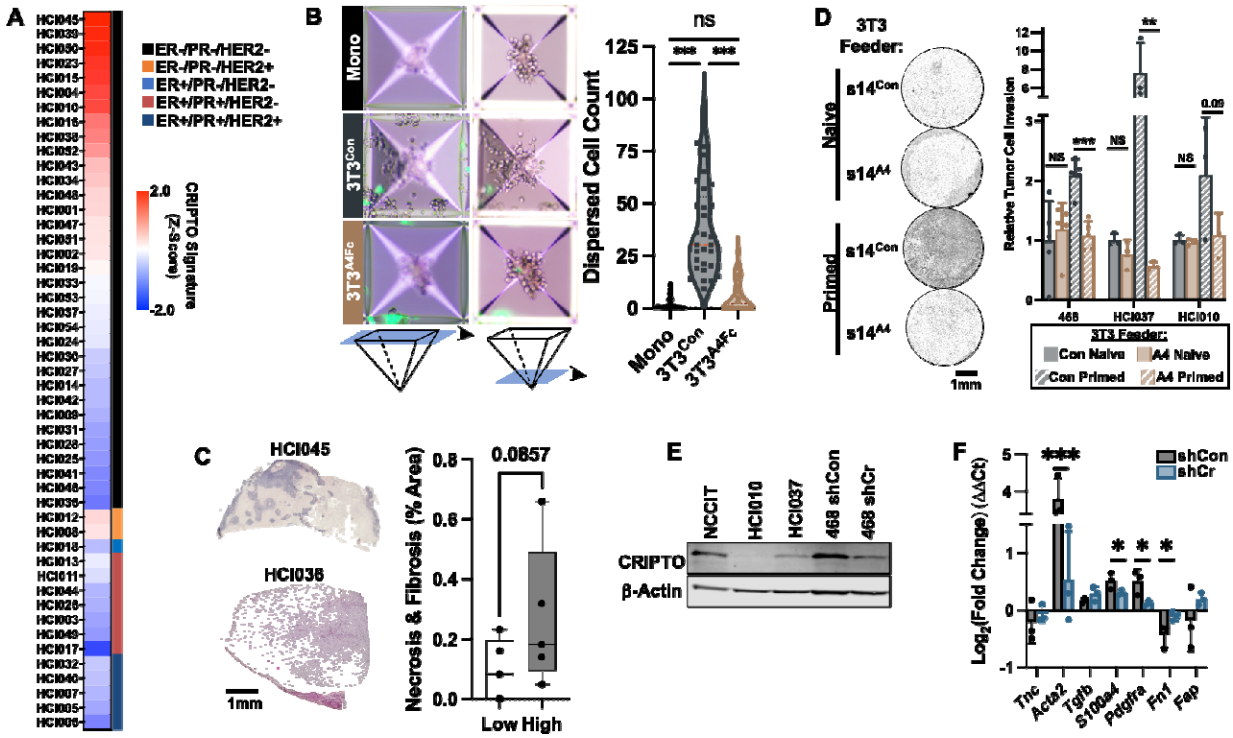

Figure 3. CRIPTO programs fibroblast differentiation through heterotypic paracrine signaling

(A) Relative CRIPTO signature across PDXs (B) Representative CRIPTO signature-high and –low PDX sections, quantification of necrotic and fibrotic area; N=5, Student's T-Test. (C) Representative photos and quantification of MDA-MB-468 spheroids grown with or without $3T3^{s14\text{-}Con}$ or $3T3^{s14\text{-}A4}$ fibroblasts in low adhesion microwells. One well=400µm. N=3 (10 microwells/biological replicate); One-way ANOVA with Tukey's multiple comparisons. (D) Transwell invasion assay of MDA-MB-468, HCI010, and HCI037 TNBC cells grown above $3T3^{s14\text{-}Con}$ or $3T3^{s14\text{-}A4}$ fibroblasts; two-way ANOVA Šidák Multiple Comparison. (E) Western blot of CRIPTO expression across cell models. (F)) RT-qPCR of CAF marker genes in 3T3 fibroblasts treated with conditioned media from shCon or shCr MDA-MB-468 cells. Fold change relative to 3T3 cells treated with autologous conditioned media; Student T-test. *P<0.05 , **P<0.01, ***P<0.001

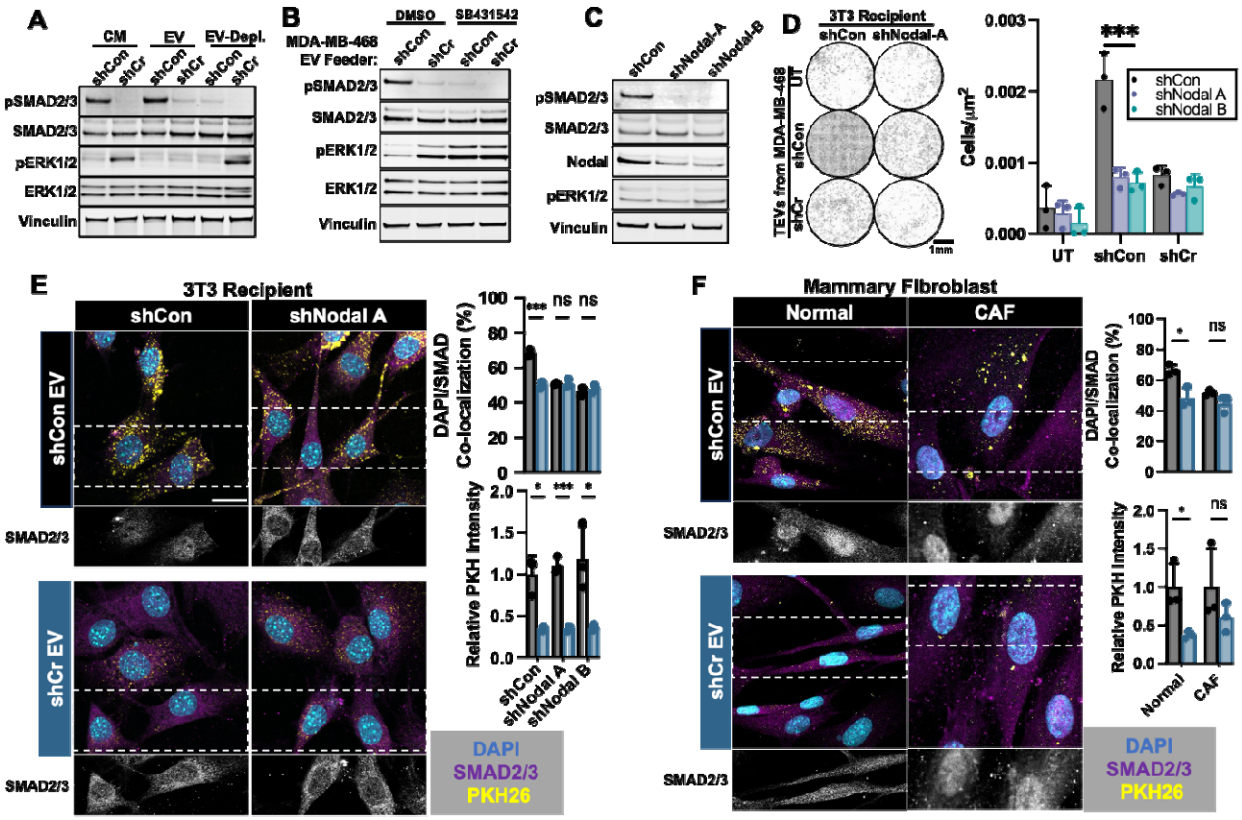

Figure 4. CRIPTO promotes SMAD activation and EV uptake in fibroblasts through discrete NODAL-dependent and –independent pathways

Western blots of 3T3s treated with (A) conditioned media (CM), TEVs or TEV-depleted media (EV-depl) collected from shCon and shCr MDA-MB-468 cells and (B) TEVs from MDA-MB-468 shCon or shCr cells in addition to treatment with SB431542 (10uM, 16hrs). (C) Western blot of shCon and NODAL knockdown (shNODAL) in 3T3s treated with TEVs from MDA-MB-468 shCon cells. (D) Invasion assay of MDA-MB-468 cells cultured above shCon or shNODAL 3T3s treated with EVs from MDA-MB-468 shCon or shCr cells. Immunocytochemistry of (E) shCon and shNodal 3T3s and (F) Primary mammary fibroblasts and CAFs treated with PKH26 labeled EVs isolated from MDA-MB-468 shCon or shCr cells. Quantification of nuclear SMAD2/3 and relative PKH intensity on the right (N=3; 4 fields of view/replicate); Holm-Šidák Multiple T-tests. Scale Bar = 20µm. *P<0.05 , **P<0.01, ***P<0.001

REFERENCES

1 Sahai, E. *et al.* A framework for advancing our understanding of cancer-associated fibroblasts. *Nat Rev Cancer* **20**, 174-186 (2020). https://doi.org:10.1038/s41568-019-0238-1

2 Freeman, D. W. *et al.* Whence CRIPTO: The Reemergence of an Oncofetal Factor in 'Wounds' That Fail to Heal. *Int J Mol Sci* **22** (2021). https://doi.org:10.3390/ijms221810164

3 Spike, B. T. *et al.* CRIPTO/GRP78 signaling maintains fetal and adult mammary stem cells ex vivo. *Stem Cell Reports* **2**, 427-439 (2014). https://doi.org:10.1016/j.stemcr.2014.02.010

4 Dublin, E., Bobrow, L., Barnes, D. & Gullick, W. Amphiregulin and cripto overexpression in breast-cancer - relationship with prognosis and clinical and molecular-variables. *Int J Oncol* **7**, 617-622 (1995). https://doi.org:10.3892/ijo.7.3.617

5 Gong, Y. P. *et al.* Overexpression of Cripto and its prognostic significance in breast cancer: a study with long-term survival. *Eur J Surg Oncol* **33**, 438-443 (2007). https://doi.org:10.1016/j.ejso.2006.10.014

6 Bianco, C. *et al.* Role of Cripto-1 in stem cell maintenance and malignant progression. *Am J Pathol* **177**, 532-540 (2010). https://doi.org:10.2353/ajpath.2010.100102

7 Balcioglu, O. *et al.* CRIPTO antagonist ALK4(L75A)-Fc inhibits breast cancer cell plasticity and adaptation to stress. *Breast Cancer Res* **22**, 125 (2020). https://doi.org:10.1186/s13058-020-01361-z

8 Klauzinska, M. *et al.* The multifaceted role of the embryonic gene Cripto-1 in cancer, stem cells and epithelial-mesenchymal transition. *Semin Cancer Biol* **29**, 51-58 (2014). https://doi.org:10.1016/j.semcancer.2014.08.003

9 Bianco, C. *et al.* A Nodal- and ALK4-independent signaling pathway activated by Cripto-1 through Glypican-1 and c-Src. *Cancer Res* **63**, 1192-1197 (2003).

10 Bianco, C. *et al.* Cripto-1 activates nodal- and ALK4-dependent and -independent signaling pathways in mammary epithelial Cells. *Mol Cell Biol* **22**, 2586-2597 (2002). https://doi.org:10.1128/MCB.22.8.2586-2597.2002

11 Gray, P. C., Harrison, C. A. & Vale, W. Cripto forms a complex with activin and type II activin receptors and can block activin signaling. *Proc Natl Acad Sci U S A* **100**, 5193-5198 (2003). https://doi.org:10.1073/pnas.0531290100

12 Gray, P. C., Shani, G., Aung, K., Kelber, J. & Vale, W. Cripto binds transforming growth factor beta (TGF-beta) and inhibits TGF-beta signaling. *Mol Cell Biol* **26**, 9268-9278 (2006). https://doi.org:10.1128/MCB.01168-06

13 Shani, G. *et al.* GRP78 and Cripto form a complex at the cell surface and collaborate to inhibit transforming growth factor beta signaling and enhance cell growth. *Mol Cell Biol* **28**, 666-677 (2008). https://doi.org:10.1128/MCB.01716-07

14 Karkampouna, S. *et al.* Oncofetal Protein CRIPTO Is Involved in Wound Healing and Fibrogenesis in the Regenerating Liver and Is Associated with the Initial Stages of Cardiac Fibrosis. *Cells* **10** (2021). https://doi.org:10.3390/cells10123325

593 15 Tchou, J. *et al.* Human breast cancer associated fibroblasts exhibit subtype specific gene
594 expression profiles. *BMC Med Genomics* **5**, 39 (2012). https://doi.org:10.1186/1755-
595 8794-5-39
596 16 Bartoschek, M. *et al.* Spatially and functionally distinct subclasses of breast cancer-
597 associated fibroblasts revealed by single cell RNA sequencing. *Nat Commun* **9**, 5150
598 (2018). https://doi.org:10.1038/s41467-018-07582-3
599 17 Sun, K. *et al.* Oxidized ATM-mediated glycolysis enhancement in breast cancer-
600 associated fibroblasts contributes to tumor invasion through lactate as metabolic
601 coupling. *EBioMedicine* **41**, 370-383 (2019).
602 https://doi.org:10.1016/j.ebiom.2019.02.025
603 18 van Niel, G., D'Angelo, G. & Raposo, G. Shedding light on the cell biology of extracellular
604 vesicles. *Nat Rev Mol Cell Biol* **19**, 213-228 (2018).
605 https://doi.org:10.1038/nrm.2017.125
606 19 Hoshino, A. *et al.* Tumour exosome integrins determine organotropic metastasis. *Nature*
607 **527**, 329-335 (2015). https://doi.org:10.1038/nature15756
608 20 Hu, C. *et al.* Exosomal Cripto-1 Serves as a Potential Biomarker for Perihilar
609 Cholangiocarcinoma. *Front Oncol* **11**, 730615 (2021).
610 https://doi.org:10.3389/fonc.2021.730615
611 21 Webber, J., Steadman, R., Mason, M. D., Tabi, Z. & Clayton, A. Cancer exosomes trigger
612 fibroblast to myofibroblast differentiation. *Cancer Res* **70**, 9621-9630 (2010).
613 https://doi.org:10.1158/0008-5472.CAN-10-1722
614 22 Mercier, I. *et al.* Human breast cancer-associated fibroblasts (CAFs) show caveolin-1
615 downregulation and RB tumor suppressor functional inactivation: Implications for the
616 response to hormonal therapy. *Cancer Biol Ther* **7**, 1212-1225 (2008).
617 https://doi.org:10.4161/cbt.7.8.6220
618 23 Yao, J., Li, S. & Wang, X. Identification of Breast Cancer Immune Subtypes by Analyzing
619 Bulk Tumor and Single Cell Transcriptomes. *Front Cell Dev Biol* **9**, 781848 (2021).
620 https://doi.org:10.3389/fcell.2021.781848
621 24 Mantile, F. *et al.* A Novel Localization in Human Large Extracellular Vesicles for the EGF-
622 CFC Founder Member CRIPTO and Its Biological and Therapeutic Implications. *Cancers*
623 *(Basel)* **14** (2022). https://doi.org:10.3390/cancers14153700
624 25 Welsh, J. A. *et al.* Minimal information for studies of extracellular vesicles (MISEV2023):
625 From basic to advanced approaches. *J Extracell Vesicles* **13**, e12404 (2024).
626 https://doi.org:10.1002/jev2.12404
627 26 Kojima, Y. *et al.* Autocrine TGF-beta and stromal cell-derived factor-1 (SDF-1) signaling
628 drives the evolution of tumor-promoting mammary stromal myofibroblasts. *Proc Natl*
629 *Acad Sci U S A* **107**, 20009-20014 (2010). https://doi.org:10.1073/pnas.1013805107
630 27 Dieters-Castator, D. *et al.* Embryonic protein NODAL regulates the breast tumor
631 microenvironment by reprogramming cancer-derived secretomes. *Neoplasia* **23**, 375-
632 390 (2021). https://doi.org:10.1016/j.neo.2021.02.004
633 28 Blanchet, M. H. *et al.* Cripto recruits Furin and PACE4 and controls Nodal trafficking
634 during proteolytic maturation. *EMBO J* **27**, 2580-2591 (2008).
635 https://doi.org:10.1038/emboj.2008.174

636 29 Blanchet, M. H. *et al.* Cripto localizes Nodal at the limiting membrane of early
637 endosomes. *Sci Signal* **1**, ra13 (2008). https://doi.org:10.1126/scisignal.1165027
638 30 Kinoshita, N., Minshull, J. & Kirschner, M. W. The identification of two novel ligands of
639 the FGF receptor by a yeast screening method and their activity in Xenopus
640 development. *Cell* **83**, 621-630 (1995). https://doi.org:10.1016/0092-8674(95)90102-7
641 31 Salmon, H. *et al.* Matrix architecture defines the preferential localization and migration
642 of T cells into the stroma of human lung tumors. *J Clin Invest* **122**, 899-910 (2012).
643 https://doi.org:10.1172/JCI45817
644 32 Karkampouna, S. *et al.* CRIPTO promotes an aggressive tumour phenotype and
645 resistance to treatment in hepatocellular carcinoma. *The Journal of Pathology* **245**, 297-
646 310 (2018). https://doi.org:10.1002/path.5083
647 33 Zoni, E. *et al.* CRIPTO and its signaling partner GRP78 drive the metastatic phenotype in
648 human osteotropic prostate cancer. *Oncogene* **36**, 4739-4749 (2017).
649 https://doi.org:10.1038/onc.2017.87
650 34 Anderton, M. J. *et al.* Induction of heart valve lesions by small-molecule ALK5 inhibitors.
651 *Toxicol Pathol* **39**, 916-924 (2011). https://doi.org:10.1177/0192623311416259
652 35 Kelly, R. K. *et al.* An antibody-cytotoxic conjugate, BIIB015, is a new targeted therapy for
653 Cripto positive tumours. *Eur J Cancer* **47**, 1736-1746 (2011).
654 https://doi.org:10.1016/j.ejca.2011.02.023
655 36 Scherer, S. D. *et al.* Breast cancer PDxO cultures for drug discovery and functional
656 precision oncology. *STAR Protoc* **4**, 102402 (2023).
657 https://doi.org:10.1016/j.xpro.2023.102402
658 37 Schindelin, J. *et al.* Fiji: an open-source platform for biological-image analysis. *Nat*
659 *Methods* **9**, 676-682 (2012). https://doi.org:10.1038/nmeth.2019
660 38 DeRose, Y. S. *et al.* Patient-derived models of human breast cancer: protocols for in vitro
661 and in vivo applications in tumor biology and translational medicine. *Curr Protoc*
662 *Pharmacol* **Chapter 14**, Unit14 23 (2013).
663 https://doi.org:10.1002/0471141755.ph1423s60
664 39 Bankhead, P. *et al.* QuPath: Open source software for digital pathology image analysis.
665 *Sci Rep* **7**, 16878 (2017). https://doi.org:10.1038/s41598-017-17204-5
666 40 Kowal, J. *et al.* Proteomic comparison defines novel markers to characterize
667 heterogeneous populations of extracellular vesicle subtypes. *Proc Natl Acad Sci U S A*
668 **113**, E968-977 (2016). https://doi.org:10.1073/pnas.1521230113
669